Nanoscience and Nanotechnology 2025, 14(1): 1-8
DOI: 10.5923/j.nn.20251401.01

Effects of Varying Growth Temperature on Optical and Structural Properties of Iron-doped Zinc Oxide Nanoparticles

Ayabei Shadrack[1], Sharon Kiprotich[1,*], John Njagi[1], Jatani Ungula[2]

[1]Department of Physical and Biological Sciences, Murang'a University of Technology, Murang'a, Kenya
[2]Department of Pure and Applied Sciences, Kenya Methodist University, Meru, Kenya

Abstract Iron-doped zinc oxide nanoparticles (Fe: ZnO NPs) have gained attention in biomedical fields due to their tunable optical properties and potential as biomedical agents. However, the influence of growth temperature on their structural integrity and luminescence performance remains unexplored. This study investigated the effect of varying growth temperature on the structural and optical properties of Fe: ZnO NPs to optimize their performance for potential bioimaging applications. Fe: ZnO NPs were synthesized using the sol-gel technique at different growth temperatures room temperature (RT), 35℃, 45℃, 55℃, 65℃, 75℃, 85℃, 95℃) and their structural and optical characterization was carried out using X-ray diffractometer (XRD), photoluminescence (PL) spectroscopy, and Ultraviolet-Visible spectrometer (UV- Vis). XRD results confirmed the retention of a single-phase hexagonal wurtzite structure, and the slight shift in peaks showed the successful incorporation of Fe. Optical properties showed systematic absorbance modulation, a blue shift, and reduced optical bandgap (3.0 eV) at 65℃. PL revealed strong UV emission peaks in the 410-470 nm region, indicating enhanced near-band-edge (NBE) emission, which was optimized at 65℃ and quenched at higher growth temperatures. Growth temperature at 65℃ yields optimum optical and structural properties, therefore not only addressing the existing knowledge gap on temperature-dependent optimization of Fe: ZnO NPs for bioimaging but also establishing a foundation for future nanomedical applications of these NPs.

Keywords Bioimaging, Fe: ZnO NPs, Sol gel synthesis, Temperature, Band gap

1. Introduction

Among several promising options for bioimaging, iron-doped zinc oxide Fe:ZnO NPshave emerged asremarkable due to their unique optical and magnetic properties [1]. The above properties render them very promising as non-invasive biomedical imaging agents, especially fluorescence imaging and magnetic resonance imaging (MRI), where materials that are highly luminescent and also biocompatible are needed [2]. To achieve their full potential in real-world applications, however, their optical and structural properties need to be finely tuned with regard to controlled synthesis conditions. The sol–gel synthesis method presents a flexible and cost-effective approach to making these nanoparticles, which can be easily fine-tuned for their structural and functional properties. This key factor that can affect the properties of Fe:ZnO nanoparticles, such as morphology and crystallinity, is the growth temperature that significantly impacts the usability of these materials towards biomedical applications. Although there is an increasing interest in Fe:ZnO NPs, the effect of growth temperature on the structural integrity and luminescent performance of these nanostructures, which are essential parameters defining the consistency of bioimaging functionality remains scanty. Numerous research papers have been conducted on synthesizing and characterizing Fe:ZnO nanoparticles for biomedical applications. For example, the work by [3] used a modified sol–gel approach to synthesize Fe-doped ZnO nanoparticles and study their structural properties. However, the effect of synthesis temperature on the nanoparticles was not considered in the investigation, leaving this as an open question for their effectiveness in bioimaging applications. Moreover, [3] identified the structural, optical, and magnetic properties of Fe-doped ZnO nanoparticles synthesized through a polymeric precursor method. They observed that tweaking the synthesis process may alter iron ions' oxidation state in the nanoparticles, hence perturbing their magnetic properties. However, the research did not study the systematic effect of growth temperature on the properties of nanoparticles, emphasizing

* Corresponding author:
Skiprotich@mut.ac.ke (Sharon Kiprotich)
Received: May 22, 2025; Accepted: Jun. 20, 2025; Published: Jul. 3, 2025
Published online at http://journal.sapub.org/nn

the need for further investigation in this field. The work by [4] focused on how iron-doped zinc oxide nanoparticles possess superior biocompatibility and multifunctional potential in various fields. Although the study outlined the biomedical application of these nanoparticles, it did not explore the role of growth temperature in influencing their biocompatibility and functional properties. These findings emphasize the crucial role of synthesis conditions in determining the intrinsic properties of Fe:ZnO nanoparticles. However, there are still few studies that investigate the correlation between synthesis temperatures and the properties of iron-doped zinc oxide nanoparticles, specifically in the context of bioimaging. In order to seal this gap, this study systematically examines how changes in growth temperature alter the structural and optical properties of Fe:ZnO NPs prepared by sol--gel method with a view of determining the conditions that would maximize their use in bioimaging applications. This study aims to fill the above gap by providing a detailed analysis of the structural and optical properties of Fe:ZnO nanoparticles as synthesized at different temperatures ranging from ambient to 95℃. In the sol–gel process, a liquid suspension called the "sol" turns into a semi-solid "gel" structure. This approach helps in synthesizing nanoparticles that are stable in terms of size and shape, as well as uniformity [5]. Although other synthesis techniques likethe hydrothermal method are efficient at producing well-crystallized ZnO nanomaterials, the fact that it can employ long reaction periods and high temperatures leads to non-uniform particle sizes and inconsistent morphologies [6]. These limitations make it challenging to acquire nanoparticles that are uniform enough for reliable bioimaging applications. Co-precipitation is singled out as a simple and low-cost technique. However, it is limited by the application of aqueous solvents, which may hinder the accuracy in the control of particle size and shape [7]. Moreover, the process may build nanoparticles with lower crystallinity, and it's prone to aggregation, which may weaken their crucial optical and structural properties that are important for the purposes of bioimaging applications [7]. Varying growth temperature during sol-gel processing can have a profound impact on the physical and chemical properties of the nanoparticles produced. Raising the temperature of synthesis typically leads to enhanced crystallinity and reduced defect density, which makes the optical properties required for bioimaging optimal [8]. Alternatively, lowering the synthesis temperature may result in nanoparticles that display enhanced surface area and different shapes, which may change their performance when interacting with biological entities [9]. The incorporation of iron in ZnO nanoparticles improves their capacity to react magnetically, qualifying them for use in the context of magnetic resonance imaging (MRI) [4]. By incorporating Fe ions into the bandgap of ZnO, it is possible to optimize its optical characteristics to address specific imaging requirements. The interactions between the growth temperature and iron doping concentration are complex, modifying the general characteristics of the nanoparticles with their joint action [10]. Research also shows that modifying the growth temperature directly influences the size, morphology, and particle dispersion of Fe:ZnO nanoparticles, hence with implications in their luminescence and magnetic responses [4]. This work seeks to understand the essence of how differences in temperatures affect the properties of Fe:ZnO nanoparticles, destined to enhance their functionality in the areas of bioimaging.

2. Methodology

Chemicals

Zinc acetate dihydrate Zn $(CH_3COO)_2\cdot \bullet H_2O$ of purity 99.9%, as a metal precursor, Diethanolamine (DEA) $C_4H_{11}NO_2$ of 99.3% purity as a complexing agent, Ethanol C_2H_5OH of 99.9% purity as a solvent for the precursor. Iron (III) nitrate nanohydrate Fe $(NO_3)_3\cdot 9H_2O$ of 98% purity, as the source of iron, Deionized water (DI) (H_2O), all supplied by Sigma Aldrich. All reagents were of analytical grade and were directly used without any special treatment.

Experimental procedure

Sol-gel technique was adopted from [11] to synthesize Fe: ZnO NPs by adding 4.4g of Zn $(CH_3COO)_2\cdot(H_2O)$ to 100 ml of ethanol in a clean beaker on a magnetic stirrer at room temperature. 2 mL of DEA was added after 15 minutes, and stirring continued until a transparent solution was formed. 0.45% Fe was added, and stirring was continued for another 30 minutes. 1.6M NaOH was added dropwise using a burette to adjust the pH to 11 with the aid of a pH meter. The contents were then transferred to a hot magnetic stirrer set at RT as the first growth temperature, and heating took place for 2hrs where a gel-like solution was formed. The solution was covered in a clean foil and left to age overnight. The gel was rinsed several times with DI before drying in an oven at 100℃ for 2hr to eliminate residual solvents and finally annealed in a muffle furnace at 500℃ for 1 hour. The sample was ground into fine NPs and kept in a sample holder for further analysis. The procedure was repeated for other growth temperatures (35℃, 45℃, 55℃, 65℃, 75℃, 85℃, 95℃).

Characterization Techniques

X-ray diffraction analysis was done using an X-ray diffractometer model ARL EQUINOX 100 with Cu-Kα radiation (λ=1.5406Å) to determine the phase purity, crystalline structure, and crystallite size of synthesized Fe: ZnO NPs. Photoluminescence spectroscopy (PL) model Infitek SPLF97 Fluorescence spectrometer was used to determine the optical emission properties and defect states of the synthesized Fe: ZnO NPs. The measurements were performed at room temperature with an excitation wavelength of 300nm. Ultra Visible spectrophotometer was used to obtain the absorbance spectra at room temperature at the wavelength range of (200-800 nm).

XRD Analysis

The X-ray diffraction pattern obtained, as shown in Figure 1, was compared with the standard reference data from the Joint Committee on Powder Diffraction Standards (JCPDS), specifically card No. 01-070-8072. All samples were synthesized

from 0.45% Fe, and the growth temperature varied from room temperature (RT), 35℃, 45℃, 55℃…….95℃, all exhibited distinct diffraction peaks corresponding to the hexagonal wurtzite phase of ZnO with no secondary phases detected. This indicates the successful incorporation of Fe^{3+} on the ZnO lattice without phase segregation.

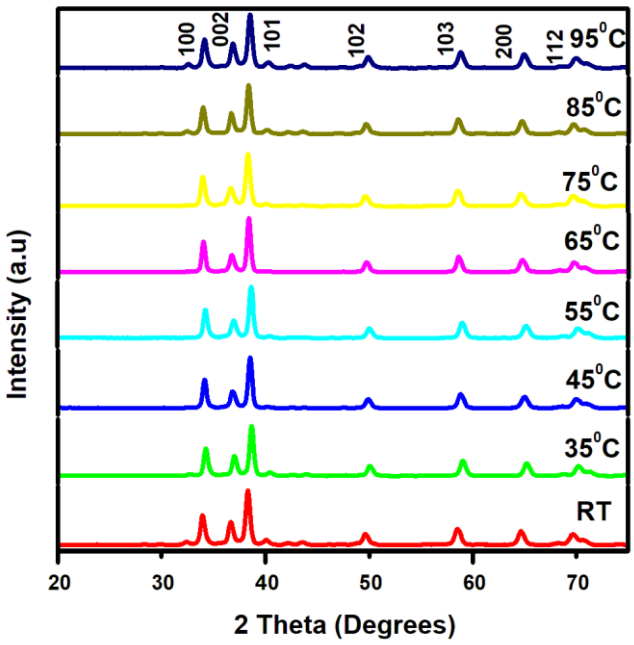

Figure 1. XRD pattern showing diffraction peaks of Fe: ZnO NPs at different growth temperatures

The most intense peak observed at plane (101) was analyzed in detail to study the crystallinity and lattice distortion across the temperature range. With increased growth temperature, a gradual intensification and sharpening of XRD peaks were observed between 55℃ and 75℃, indicating enhanced crystallinity due to atomic diffusion and grain growth at high temperatures [12]. This trend is consistent with previously reported findings where elevated growth temperatures promoted crystallite growth and reduced structural disorder on Fe: ZnO NPs [13].

The interplanar d spacing and the average crystallite size were calculated using Bragg's equation and Debye-Scherrer formula, respectively. Equation 1 gives Bragg's equation [13], Equation 2 gives the Debye-Scherrer formula [14].

$$n\lambda = 2d \sin\theta \quad (1)$$

Where n represents the order of diffraction (n=1), λ is the wavelength of the incident rays, d is the interplanar spacing between crystal planes, and θ is Bragg's angle, which is half of the 2θ.

$$D = \frac{0.9\lambda}{\beta COS\ \theta} \quad (2)$$

Where D is the crystallite size in (nm), λ is the wavelength 1.5406Å (Cu Kα radiation) of X-rays (1.5406Å), β is the full width at half maximum (FWHM) of the peak in radians, and θis the Bragg angle.

The average crystallite size in Table 1 indicated adecrease from around 22.75 nm at room temperature to approximately 18.26 nm at 65℃, followed by a decrease at higher temperatures. These findings are corroborated by prior reports, [3] a similar trend was observed on Fe: ZnO NPs synthesized via hydrothermal methods, where the crystallite size decreased with growth temperature. Similarly, [15] studied the effect of temperature on the ZnO nanostructures, confirmed that a decrease in growth temperature led to better crystallinity and sharper XRD peaks attributed to better grain boundary diffusion in the nucleation stage. The results also indicate that as the growth temperature increases, the FWHM increases, corresponding to adecrease in crystallite size. This trend suggests enhanced crystallinity and grain growth at elevated temperatures, as reported by [16] who discovered that higher growth temperatures improved the crystal quality of ZnO NPs, inducing a reduction in the FWHM value. The systematic shift in 2θ values to higher angles shows a decrease in lattice spacing (d), indicating a compressive strain within the ZnO lattice. Such strain is introduced when Fe^{3+}substitutes Zn^{2+}, causing lattice contraction. A similar trend has been reported, for example, [17] discovered that Fe: ZnO showed the same 2θ shifts to higher values with doping, indicating successful incorporation and lattice distortion.

Table 1. FWHM and crystallite size values of all Fe: ZnO NPs samples at different growth temperatures

Plane	100	002	101	102	103	200	Crystallite Size D (nm)
	FWHM (Degrees)						
Room Temperature (RT)	0.41084	0.37278	0.38771	0.53994	0.58407	0.60361	22.75
35℃	0.42342	0.39934	0.40320	0.51211	0.54131	0.56386	21.18
45℃	0.44476	0.43526	0.41640	0.55472	0.57502	0.63763	20.65
55℃	0.40431	0.46841	0.42706	0.55881	0.57374	0.64505	19.88
65℃	0.34401	0.44125	0.44531	0.49859	0.50133	0.56886	18.26
75℃	0.41378	0.43075	0.42767	0.60631	0.61927	0.69273	19.09
85℃	0.38416	0.39416	0.40130	0.50887	0.53819	0.54427	21.64
95℃	0.43184	0.42797	0.38518	0.59843	0.58976	0.60676	22.69

Table 2. 2θ, d spacing, and lattice parameters a and c values of all planes for Fe: ZnO NPs at different growth temperatures

Plane	100	002	101	102	103	200	Average d-Spacing	a	c
	2θ (Degrees)								
Room Temperature	33.990	36.714	38.358	49.660	58.549	64.677	2.345	4.5646	4.8917
35℃	34.300	37.060	38.713	50.097	58.047	65.228	2.324	4.5246	4.8476
45℃	34.186	36.932	38.576	49.937	58.867	65.030	2.332	4.5392	4.8636
55℃	34.303	37.041	38.703	50.085	59.040	65.208	2.324	4.5242	4.8500
65℃	34.052	36.802	38.422	49.755	58.657	64.802	2.340	4.5566	4.8804
75℃	34.010	36.719	38.376	49.677	58.577	64.697	2.344	4.5620	4.8911
85℃	34.016	36.765	38.400	49.717	58.602	64.747	2.342	4.5612	4.8852
95℃	34.177	36.919	38.566	49.922	58.844	64.996	2.333	4.5404	4.8655

Estimation of strain and Dislocation density

The strain induced in NPs due to crystal imperfections and distortion was calculated using the Williamson-Hall method, shown by equation 3, while dislocation density was calculated using the Williamson-Smallman relation as shown by equation 4.

$$\varepsilon = \frac{\beta}{4 \tan \theta} \quad (3)$$

Where ε represents the microstrain, β is the FWHM in radians, and θ is the diffraction angle of the most intense peak (101).

$$\delta = \frac{1}{D^2} \quad (4)$$

Where δ is the dislocation density in nm^{-2}, and D is the crystallite size in (nm).

Table 3. Calculated micro-strain and dislocation density at peak (101) for Fe: ZnO NPs at varying growth temperatures

Growth temperature ℃	Micro-strain	Dislocation Density (nm^{-2})
Room Temperature (RT)	0.0051	0.0023
35℃	0.0047	0.0021
45℃	0.0048	0.0019
55℃	0.0049	0.0016
65℃	0.0044	0.0017
75℃	0.0052	0.0022
85℃	0.0047	0.0019
95℃	0.0051	0.0022

From the results in Table 3, Fe-doped ZnO NPs synthesized at various growth temperatures indicate that there is an inverse relationship between crystallite size and both microstrain and dislocation density. At higher growth temperature of 55℃, the crystallite size increases, but the microstrain and dislocation density decrease as shown in Figure 2, revealing improved crystallinity and fewer defects. This is in concordance with the work of [18] who noted that as the substrate temperature is increased during deposition of Fe-doped ZnO NPs, the crystallite size increases while microstrain and dislocation density decrease due to enhanced atomic diffusion and grain growth at higher temperatures. Moreover, [19], observed reduced micro strain and dislocation density in Fe-doped ZnO nanoparticles decreased when the crystallite size increased due to substitution of Fe^{3+} entering the ZnO lattice, causing the lattice relaxation.

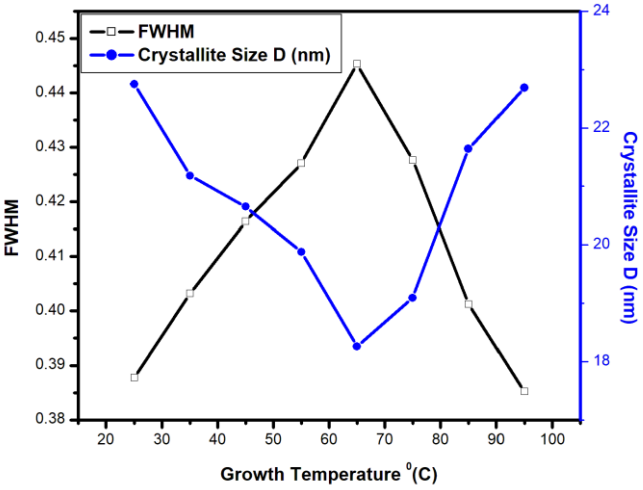

Figure 2. Variation of FWHM and Crystallite size D (nm) of Fe: ZnO NPs at varying growth temperatures

The XRD pattern demonstrated that the desired substitutional doping of Fe^{3+} in the ZnO lattice was achieved at all temperatures, and no secondary phases were formed. Interestingly, the lowest crystallite size (18.26 nm), microstrain, and lighter dislocation density were obtained at a synthesis temperature of 65℃, which is suggestive of a well-ordered crystalline structure. In comparison to literature, this low temperature optimization is a new path to high-quality Fe:ZnO NPs through sol-gel synthesis. These structural features directly contribute to the optical properties and stability, which justify their application in bioimaging, where the integrity of the crystals and low density of defects are paramount.

Photoluminescence analysis

Figure 3 shows the PL spectra and of Fe: ZnO NPs at an excitation wavelength of 300nm, recorded at room temperature at an emission range of 250nm to 800nm. This analysis aimed to assess the influence of different growth temperatures on the deep-level effect emissions and band edge emission of ZnO.

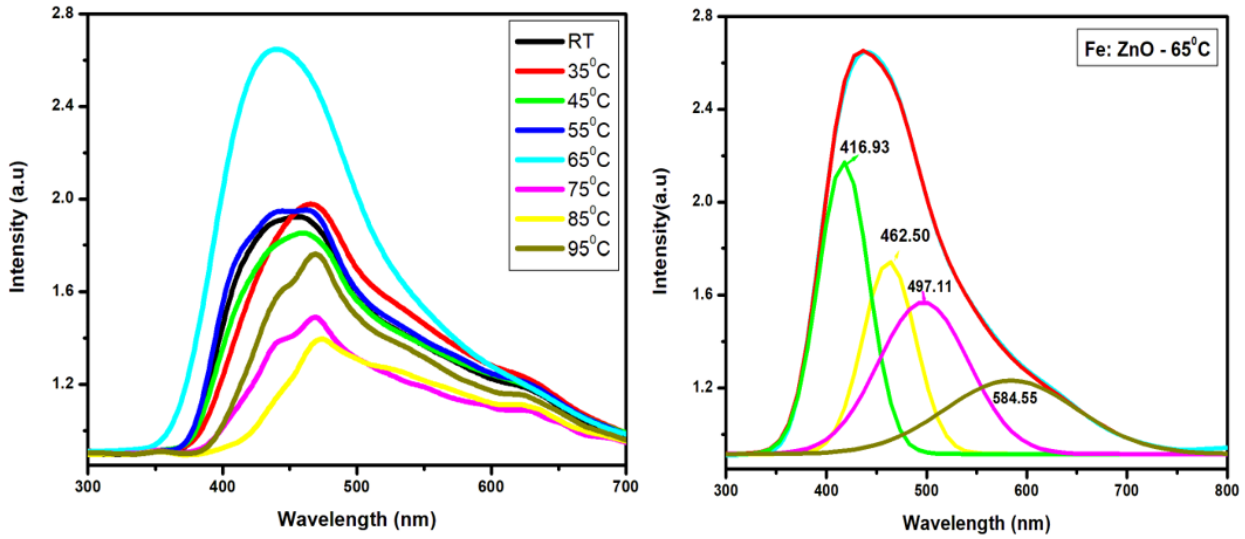

(a) **(b)**

Figure 3. (a) Photoluminescence spectra (PL) of Fe: ZnO NPs at different growth temperatures and (b) Deconvolution of Fe: ZnOat 65℃

PL spectra suggest that Fe-doped ZnO nanoparticles depict a temperature-dependent shift in both the emission wavelength and intensity. At lower growth temperatures (RT to 55℃), the emission peaks were observed at 460–471 nm with moderate intensity ranging from 0.76 to 0.88a.u, as shown in Table 4, which can be attributed to standard excitonic and defect-level transitions. Importantly, at 65℃, the intensity of the PL reached 1.51 a.u and the emission wavelength shifted to 454.21 nm, indicating that the crystallinity increased and non-radiative defects were minimized. At higher temperatures (75℃ to 95℃), a red shift to 483–485 nm and a decrease in intensity was found, which could be attributed to the generatively deep-level defects and non-radiative recombination. The findings match previous research; [20] found increased PL intensity due to better crystallinity and reduced point defects in ZnO NPs synthesized at higher growth temperatures around 60℃. Moreover, [21] investigated the ZnO nanocrystals and observed that when samples were synthesized at high growth temperatures (70℃), PL red shifts and lower intensity were recorded due to defect clustering and thermal-induced stress. The Gaussian deconvolution of the photoluminescence (PL) spectra of Fe: ZnO NPs prepared at different growth temperatures demonstrated in Figure 3b shows four distinctive emission bands, which are associated with certain defects in the ZnO lattice. These emissions are concentrated around 417 nm, 463 nm, 497 nm, and 585 nm. The 417 nm emission is associated with zinc interstitials (Zn_i), which are shallow donor defects responsible for the near band-edge emissions (NBE). The peak at 463 nm is attributed to oxygen vacancies (V_O), commonly linked to green luminescence of ZnO. The 497 nm emission is associated with oxygen interstitials (O_i), and the 585 nm band is due to deep-level trap states resulting from Fe^{3+} ions [22]. These results match previous work on Fe: ZnO NPs. For example, similar defect-related emissions in Fe-doped ZnO NPs were reported by [22] who specified peaks corresponding to Zn_i, V_O, and Fe^{3+} trap states. The growth temperature dependence of PL intensity and peak position variation suggests that heat treatment has a controlling role on defect formation and distribution. The best growth temperature at about 65℃ leads to increased PL intensity, possibly because of the optimal defect concentration and crystallinity balance. Elevated temperatures can cause an increase in the presence of non-radiative recombination centers, which can decrease PL efficiency [21].

Table 4. Emission wavelengths and PL intensities of Fe:ZnO NPs at different growth temperatures

Growth temperature ℃	Emission wavelength (nm)	PL Intensity
RT	463.00	0.80492
35℃	460.75	0.83990
45℃	471.23	0.76596
55℃	463.74	0.88127
65℃	454.21	1.5083
75℃	483.39	0.43535
85℃	439.15	0.39656
95℃	485.64	0.66529

Photoluminescence spectra showed an apparent temperature dependency in the emission intensity and wavelength, with 65℃ yielding the most intensive NBE emission at 454.21nm. This improvement is ascribed to the better crystallinity and lower non-radiative recombination owing to the optimum defect concentrations. Deconvolution verified emissions attributed to Zn_i, V-O, O_i, and Fe^{3+} states reflecting the delicate balance between growth temperature and defect formation. In comparison to current reports, the present work offers the unlikely, systematic adjustment of emission behavior over a low temperature range, revealing an exact synthesis window producing bioimaging-ready nanoparticles. These findings illustrate how well-regulated growth temperature conditions can produce Fe:ZnO NPs with outstanding optical characteristics that are prerequisite in high-resolution, low-toxicity bioimaging platforms.

Optical analysis

Figure 4 shows UV–Vis absorbance spectra of the Fe-doped ZnO NPs synthesized at varying growth temperatures. The spectra reveal that the position of the absorption edge changed with the growth temperature. At lower growth temperatures (from 25℃ to 350℃), the absorption edge moves to lower energies (blue shift), which means that the bandgap energy increases. This blue shift can be attributed to the Burstein–Moss effect, where an increase in the carrier concentration in the conduction band leads to the occupation of the lower energy levels, thus increasing the energy bandgap [13]. When the growth temperature rises above 45℃, a shift in the absorption edge to a longer wavelength is observed, indicating a decrease in the bandgap energy. This red shift can be attributed to better crystallinity and fewer defects, which decreases the bandgap [23].

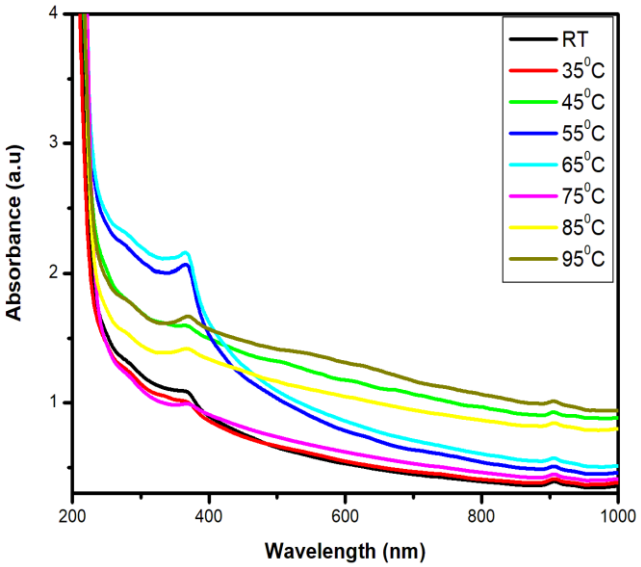

Figure 4. Ultra Violet Visible (UV Vis) absorbance spectra of Fe: ZnO NPs at varying growth temperatures

To quantitatively calculate the optical bandgap (E_g), Tauc plots were constructed, and the Tauc relation was used. Equation 5 gives the Tauc relation [24]

$$(\alpha h\nu)^n = A(h\nu - E_g) \quad (5)$$

Where α is the absorption coefficient, $h\nu$ is the photon energy, E_g is the optical bandgap, A is a constant, while n depends on the number of electronic transitions. $n=\frac{1}{2}$ for direct allowed transitions, while n = 2 for indirect allowed transitions. Since ZnO is a direct bandgap semiconductor, $n=\frac{1}{2}$ was used. The Tauc plot was obtained by plotting $(\alpha h\nu)^2$ against photon energy ($h\nu$), and the optical band gap was obtained by extrapolating the linear portion of the curve to the x-axis where $(\alpha h\nu)^2 = 0$. Figure 5 shows the optical band gaps obtained through extrapolation and summarized in Table 5.

By extending the linear portions of the Tauc plot to the photon energy axis, a clear dependence of band gap energies on the synthesis temperature is seen. The band gap was found to vary between the reference sample with room temperature synthesized Fe:ZnO (4.43 eV) to the highest value of 4.88 eV at 95℃, and decreased sharply to a minimum of 3.0 eV at 65℃. This non-monotonic behavior indicates the possibility of a relationship between the growth temperature, crystal quality, particle size, and dopant incorporation. The greater increase of the band gap at lower temperatures can be attributed to the quantum confinement effects by smaller crystallite size, which leads to a rise in the energy bandgap because of the restriction of motion of the charge carriers; This effect has been reported by [25]. However, it should be noted that the observed blue shift at the low-temperature side can also partially originate from the Burstein–Moss effect, where the increasing carrier concentration, perhaps due to excess Fe doping, immerses the Fermi level in the conduction band and, thus, increases the optical gap [8].

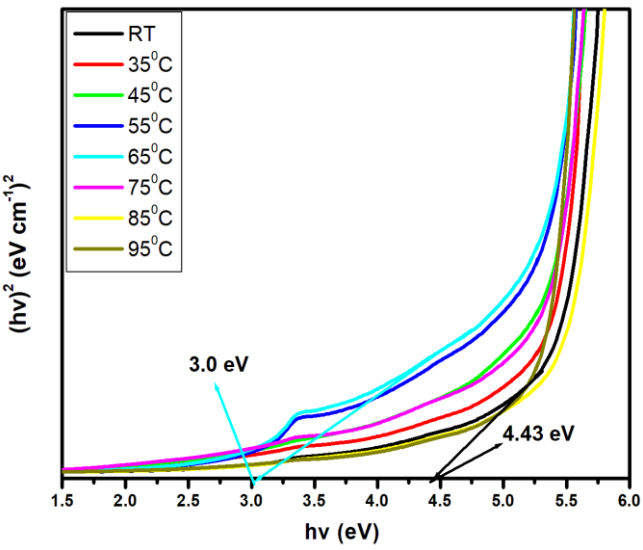

Figure 5. Tauc plot showing extrapolated band gaps of Fe: ZnO NPs at different growth temperatures

The significant reduction in the band gap, as shown in Table 5 at about 55–65℃, could also imply structural changes or increased surface defects that create mid-gap states that enable absorption sub-bandgap, thereby lowering the optical band gap [26]. A similar trend has also been observed by [27] in Fe-doped ZnO NPs synthesized by hydrothermal and sol-gel methods, where the thermal treatment optimized the defects and homogeneity of Fe in ZnO lattice, resulting in the reduced band gap in the range of 3.2-3.6 eV.

Table 5. Band gap values of Fe: ZnO NPs at varying growth temperatures

Growth Temperature	Band Gap (eV)
RT	4.43
35℃	4.12
45℃	3.84
55℃	3.25
65℃	3.0
75℃	4.12
85℃	4.60
95℃	4.88

The overall tunable band gaps found in this study (3.0–4.88 eV) are wider than those already reported, which suggests the ability to achieve a significant level of structural and electronic variation by controlling the temperature. The onset of the bandgap of 3.0 eV at 65℃ coincides with the optimized structural quality and the intensity of the PL emission, confirming the suitability of this temperature as the one that can be used in bioimaging practices. That non-monotonic behavior of the bandgap was explained to be caused by a combination of the effects of quantum confinement at low temperatures, the Burstein-Moss shift associated with carrier accumulation, and defect-state absorption at the band edges. This wide spectral tunability is hardly found and makes Fe: ZnO NPs more useful in Biomedical imaging systems with customized optical behavior. This tunability will be particularly important when applying Fe:ZnO nanocomposites for UV photodetectors, photocatalysts, and transparent conduction oxides; these applications have distinct band gap impedances that are critical to device performance [28].

3. Conclusions

Herein, Fe: ZnO NPs at varying growth temperatures were successfully synthesized via the sol-gel technique, which offered a cost-effective and simple controllable route for tuning the structural and optical properties. XRD analysis confirmed the presence of the hexagonal wurtzite structure of ZnO with no secondary phases. The average crystallite size estimated using the Debye-Scherrer formula decreased from 22.75 nm at RT to 18.26 nm at 65℃. PL investigation revealed 65℃ with the highest intensity at 1.51 a.u and the emission wavelength shifted to 454.21 nm, indicating that the crystallinity increased and non-radiative defects were minimized. UV- Vis absorption analysis and Tauc plots confirmed that the bandgap can be tuned through variation of the growth temperature. Optical bandgap analyzed for all samples was found to decrease initially from 4.43 eV at RT to as low as 3.0 eV at 65℃ and then increased slightly for higher growth temperatures due to the Burstein-Moss effect. By addressing the research gaps identified in earlier studies, the findings of this study enhance the understanding of how optimizing growth temperature, the synthesis can effectively be used to tailor Fe:ZnO nanoparticles towards biocompatibility and specificity. These findings offer a strong foundation for developing modified advanced nanoparticles for non-invasive, high-resolution bioimaging.

ACKNOWLEDGEMENTS

The authors wish to thank Murang'a University of Technology for offering access to various synthesis and characterization techniques for this research.

Conflict of Interest

The authors declare no conflict of interest.

REFERENCES

[1] M. Carofiglio, S. Barui, V. Cauda, and M. Laurenti, "Doped Zinc Oxide Nanoparticles: Synthesis, Characterization and Potential Use in Nanomedicine," *Appl. Sci.*, vol. 10, no. 15, p. 5194, Jul. 2020, doi: 10.3390/app10155194.

[2] Z. L. Wang, "Zinc oxide nanostructures: growth, properties and applications," *J. Phys. Condens. Matter*, vol. 16, no. 25, pp. R829–R858, Jun. 2004, doi: 10.1088/0953-8984/16/25/R01.

[3] F. F. H. Aragón *et al.*, "Evidence of progressive Fe^{2+} to Fe^{3+} oxidation in Fe^{2+}-doped ZnO nanoparticles," *Mater. Adv.*, vol. 4, no. 5, pp. 1389–1402, 2023, doi: 10.1039/d3ma00053b.

[4] M. Foyshal, M. F. Kabir, A. Islam, J. Ferdousy, M. R. Islam, and M. M. Rahman, "Enhanced Biocompatibility and Multifunctional Properties of Iron-Doped Zinc Oxide Nanoparticles for Applications," Oct. 18, 2023. doi: 10.21203/rs.3.rs-3426239/v1.

[5] R. S. Kate, S. A. Khalate, and R. J. Deokate, "Overview of nanostructured metal oxides and pure nickel oxide (NiO) electrodes for supercapacitors: A review," *J. Alloys Compd.*, vol. 734, pp. 89–111, Feb. 2018, doi: 10.1016/j.jallcom.2017.10.262.

[6] M. Z. Hossain, S. M. A. Nayem, Md. S. Alam, Md. I. Islam, G. Seong, and A.-N. Chowdhury, "Hydrothermal ZnO Nanomaterials: Tailored Properties and Infinite Possibilities," *Nanomaterials*, vol. 15, no. 8, p. 609, Apr. 2025, doi: 10.3390/nano15080609.

[7] S. Fabbiyola, L. J. Kennedy, U. Aruldoss, M. Bououdina, A. A. Dakhel, and J. Judith Vijaya, "Synthesis of Co-doped ZnO nanoparticles via co-precipitation: Structural, optical and magnetic properties," *Powder Technol.*, vol. 286, pp. 757–765, Dec. 2015, doi: 10.1016/j.powtec.2015.08.054.

[8] S. Chakrabarti *et al.*, "Sonochemical Synthesis and Characterization of Iron (Fe) Doped Zinc Oxide (ZnO) Nanoparticles," 2016, pp. 55–61.

[9] S. Kumari *et al.*, "A comprehensive review on various techniques used for synthesizing nanoparticles," *J. Mater. Res. Technol.*, vol. 27, pp. 1739–1763, Nov. 2023, doi: 10.1016/j.jmrt.2023.09.291.

[10] S. H. Zyoud *et al.*, "Superior photocatalytic degradation of pharmaceuticals and antimicrobial Features of iron-doped zinc oxide sub-microparticles synthesized via laser-assisted chemical bath technique," *Results Eng.*, vol. 24, p. 102875, Dec. 2024, doi: 10.1016/j.rineng.2024.102875.

[11] A. Vishwakarma, "Synthesis of Zinc Oxide Nanoparticle by Sol-Gel Method and Study its Characterization," *Int. J. Res. Appl. Sci. Eng. Technol.*, vol. 8, no. 4, pp. 1625–1627, Apr. 2020, doi: 10.22214/ijraset.2020.4265.

[12] N. Mufti *et al.*, "The Effect of Growth Temperature on The

Characteristics Of ZnO Nanorods And Its Optical Properties," *J. Phys. Conf. Ser.*, vol. 1057, p. 012005, Jul. 2018, doi: 10.1088/1742-6596/1057/1/012005.

[13] O. H. Abd-Elkader, M. Nasrallah, L. Aleya, and M. Nasrallah, "Biosynthesis, Optical and Magnetic Properties of Fe-Doped ZnO/C Nanoparticles," *Surfaces*, vol. 6, no. 4, pp. 410–429, Oct. 2023, doi: 10.3390/surfaces6040028.

[14] Department of Physical and Biological Sciences, Murang'a University of Technology, PO BOX 75, Murang'a 10200, Kenya and J. Jepngetich, "Effects of Ag Doping Concentrations on Structural and Optical Properties of Citrus Reticulata Capped ZnO Nanoparticles," *J. Nanosci. Res. Rep.*, pp. 1–7, Apr. 2025, doi: 10.47363/JNSRR/2025(7)176.

[15] D. Dasuki, K. Habanjar, and R. Awad, "Effect of Growth and Calcination Temperatures on the Optical Properties of Ruthenium-Doped ZnO Nanoparticles," *Condens. Matter*, vol. 8, no. 4, p. 102, Nov. 2023, doi: 10.3390/condmat8040102.

[16] A. G. Kaningini *et al.*, "Effect of Optimized Precursor Concentration, Temperature, and Doping on Optical Properties of ZnO Nanoparticles Synthesized via a Green Route Using Bush Tea (*Athrixia phylicoides* DC.) Leaf Extracts," *ACS Omega*, vol. 7, no. 36, pp. 31658–31666, Sep. 2022, doi: 10.1021/acsomega.2c00530.

[17] T. Srinivasulu, K. Saritha, and K. T. R. Reddy, "Synthesis and characterization of Fe-doped ZnO thin films deposited by chemical spray pyrolysis," *Mod. Electron. Mater.*, vol. 3, no. 2, pp. 76–85, Jun. 2017, doi: 10.1016/j.moem.2017.07.001.

[18] P. L. Hadimani, S. S. Ghosh, and A. Sil, "Preparation of Fe doped ZnO thin films and their structural, magnetic, electrical characterization," *Superlattices Microstruct.*, vol. 120, pp. 199–208, Aug. 2018, doi: 10.1016/j.spmi.2018.05.029.

[19] L. Amin, "Influence of Fe substitution on structural and morphological properties of Zn1-xFexO thin films for varies applications," *Sohag J. Sci.*, vol. 0, no. 0, pp. 0–0, Jan. 2023, doi: 10.21608/sjsci.2022.153658.1017.

[20] U. R. Gudla *et al.*, "Optical and luminescence properties of pure, iron-doped, and glucose capped ZnO nanoparticles," *Results Phys.*, vol. 19, p. 103508, Dec. 2020, doi: 10.1016/j.rinp.2020.103508.

[21] F. B. Dejene, "Characterization of low-temperature-grown ZnO nanoparticles: The effect of temperature on growth," *J. Phys. Commun.*, vol. 6, no. 7, p. 075011, Jul. 2022, doi: 10.1088/2399-6528/ac8049.

[22] N. Mohamed Basith, J. Judith Vijaya, L. John Kennedy, M. Bououdina, R. Shenbhagaraman, and R. Jayavel, "Influence of Fe-Doping on the Structural, Morphological, Optical, Magnetic and Antibacterial Effect of ZnO Nanostructures," *J. Nanosci. Nanotechnol.*, vol. 16, no. 2, pp. 1567–1577, Feb. 2016, doi: 10.1166/jnn.2016.10756.

[23] M. Suchea, S. Christoulakis, M. Katharakis, N. Vidakis, and E. Koudoumas, "Influence of thickness and growth temperature on the optical and electrical properties of ZnO thin films," *Thin Solid Films*, vol. 517, no. 15, pp. 4303–4306, Jun. 2009, doi: 10.1016/j.tsf.2008.11.143.

[24] N. Madkhali, "Analysis of Structural, Optical, and Magnetic Properties of (Fe,Co) Co-Doped ZnO Nanoparticles Synthesized under UV Light," *Condens. Matter*, vol. 7, no. 4, p. 63, Nov. 2022, doi: 10.3390/condmat7040063.

[25] S. Ilican, Y. Özdemir, M. Caglar, and Y. Caglar, "Temperature dependence of the optical band gap of sol-gel derived Fe-doped ZnO films," *Optik*, vol. 127, no. 20, pp. 8554–8561, Oct. 2016, doi: 10.1016/j.ijleo.2016.06.074.

[26] Munirah, Z. R. Khan, A. Aziz, Mohd. S. Khan, and M. U. Khandaker, "Influence of zinc concentration on band gap and sub-band gap absorption on ZnO nanocrystalline thin films sol-gel grown," *Mater. Sci.-Pol.*, vol. 35, no. 1, pp. 246–253, Feb. 2017, doi: 10.1515/msp-2017-0039.

[27] N. Üzar, "Effect of 15% Fe doping on the structural, optical, electrical, and thermoelectric properties of ZnO thin films," *Phys. B Condens. Matter*, vol. 704, p. 417045, May 2025, doi: 10.1016/j.physb.2025.417045.

[28] S. L. Jenish *et al.*, "Improved optical and electrical properties of Fe doped ZnO nanostructures facilely deposited by low-cost SILAR method for photosensor applications," *Surf. Interfaces*, vol. 31, p. 102071, Jul. 2022, doi: 10.1016/j.surfin.2022.102071.